



ARTICLE

Species differences in the CYP3A-catalyzed metabolism of TPN729, a novel PDE5 inhibitor

Qian-qian Tian^{1,2}, Yun-ting Zhu^{1,2}, Xing-xing Diao¹, Xiang-lei Zhang¹, Ye-chun Xu¹, Xiang-rui Jiang³, Jing-shan Shen³, Zhen Wang³ and Da-fang Zhong^{1,2}

TPN729 is a novel phosphodiesterase 5 (PDE5) inhibitor used to treat erectile dysfunction in men. Our previous study shows that the plasma exposure of metabolite M3 (N-dealkylation of TPN729) in humans is much higher than that of TPN729. In this study, we compared its metabolism and pharmacokinetics in different species and explored the contribution of its main metabolite M3 to pharmacological effect. We conducted a combinatory approach of ultra-performance liquid chromatography/quadrupole time-of-flight mass spectrometry-based metabolite identification, and examined pharmacokinetic profiles in monkeys, dogs, and rats following TPN729 administration. A remarkable species difference was observed in the relative abundance of major metabolite M3: i.e., the plasma exposure of M3 was 7.6-fold higher than that of TPN729 in humans, and 3.5-, 1.2-, 1.1-fold in monkeys, dogs, and rats, respectively. We incubated liver S9 and liver microsomes with TPN729 and CYP3A inhibitors, and demonstrated that CYP3A was responsible for TPN729 metabolism and M3 formation in humans. The inhibitory activity of M3 on PDE5 was 0.78-fold that of TPN729 (The IC_{50} values of TPN729 and M3 for PDE5A were 6.17 ± 0.48 and 7.94 ± 0.07 nM, respectively.). The plasma protein binding rates of TPN729 and M3 in humans were 92.7% and 98.7%, respectively. It was astonishing that the catalyzing capability of CYP3A4 in M3 formation exhibited seven-fold disparity between different species. M3 was an active metabolite, and its pharmacological contribution was equal to that of TPN729 in humans. These findings provide new insights into the limitation and selection of animal model for predicting the clinical pharmacokinetics of drug candidates metabolized by CYP3A4.

Keywords: PDE5 inhibitor; TPN729; M3; CYP3A4; species difference; pharmacokinetics; metabolite identification

Acta Pharmacologica Sinica (2021) 42:482–490; <https://doi.org/10.1038/s41401-020-0447-x>

INTRODUCTION

Erectile dysfunction (ED) represents a serious health concern that can affect the quality of life of patients [1, 2]. In clinical practice, phosphodiesterase 5 (PDE5) inhibitors have been used for the treatment of ED. Sildenafil (Fig. 1) is the first-line PDE5 inhibitor for most men with ED. It has been used in clinic for over 20 years [3].

TPN729 (Fig. 1) is novel PDE5 inhibitor for ED treatment, which is in phase II clinical trials in China. TPN729 exhibits high efficiency for ED treatment, with 2.5-fold greater affinity than sildenafil. The greater selectivity for PDE5 over the other PDE isozymes highlights TPN729 as an effective PDE5 inhibitor with fewer adverse effects and better tolerance [4].

The molecular structure of TPN729 is similar to that of sildenafil. There have been many reports on the metabolism of sildenafil. In humans, the demethylation of sildenafil to its principal circulating metabolite, UK-103,320 (Fig. 1), is largely mediated by cytochrome P450 3A4 (CYP3A4) [5, 6]. The similarity index indicated that the metabolism of sildenafil in mice was highly analogous to that in humans when compared with other animals [7]. The formation of UK-103,320 was observed in mice, rabbits, rats, dogs, and humans,

and the ratios of $C_{\max \text{ UK-103,320}}/C_{\max \text{ sildenafil}}$ were 0.21, 1.0, 0.14, and 0.48 in mice, male rats, dogs, and humans, respectively [5, 8]. Udenafil (Fig. 1) is another PDE5 inhibitor, which is also an isomer of TPN729. The main active metabolite of udenafil, DA-8164 (Fig. 1), is produced by CYP3A [9, 10]. The formation of DA-8164 in mice, rats, dogs, and humans has been investigated, and the $AUC_{\text{DA-8164}}/AUC_{\text{udenafil}}$ ratios after oral administration were 2.99, 2.67, 0.065, and 1.39, respectively [11]. The identification of TPN729 metabolites in humans and its pharmacokinetic profiles in humans, rats, and dogs have been previously reported [12–14]. A significant phenomenon was observed, in which the plasma exposure of metabolite M3 (Fig. 1) in humans was found to be 7.6-fold higher than that of TPN729 [15]. However, thus far, no studies have been conducted on the $AUC_{\text{M3}}/AUC_{\text{TPN729}}$ ratios in different species, and the main enzymes involved in TPN729 metabolism and M3 formation in different species are still unclear.

The objectives of the current work are: (1) to compare the metabolism and pharmacokinetics of TPN729 in humans, monkeys, dogs, and rats; (2) to investigate the major enzymes that contribute to TPN729 metabolism and M3 formation in different species; and (3) to explore the pharmacological activity of M3.

¹State Key Laboratory of Drug Research, Shanghai Institute of Materia Medica, Chinese Academy of Sciences, Shanghai 201203, China; ²University of Chinese Academy of Sciences, Beijing 100049, China and ³CAS Key Laboratory for Receptor Research, Shanghai Institute of Materia Medica, Chinese Academy of Sciences, Shanghai 201203, China
Correspondence: Zhen Wang (wangzhen@simm.ac.cn) or Da-fang Zhong (dfzhong@simm.ac.cn)

Received: 30 November 2019 Accepted: 17 May 2020

Published online: 24 June 2020

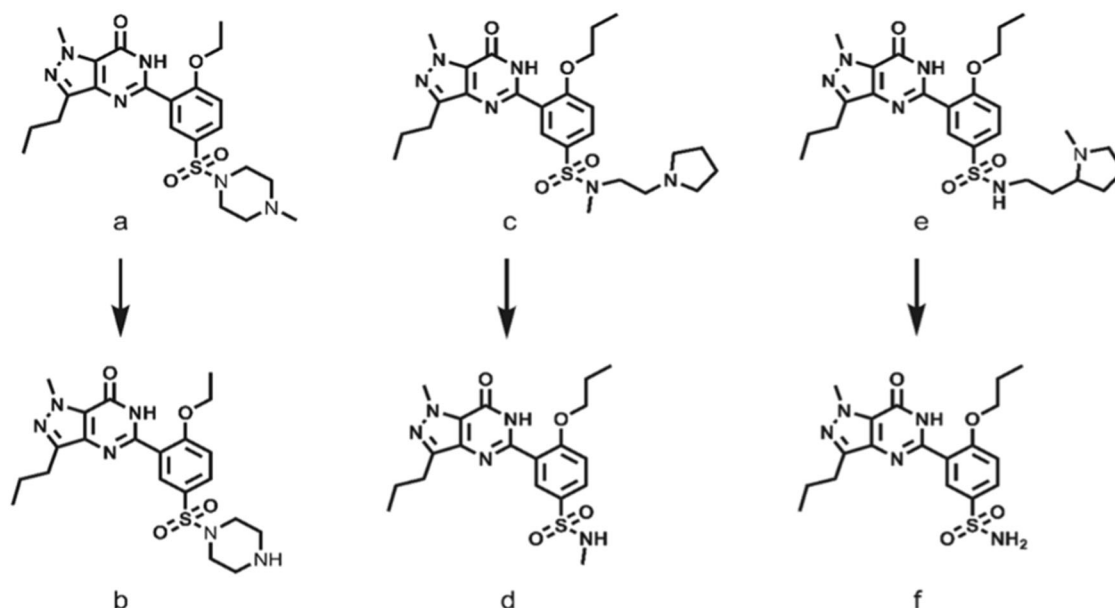


Fig. 1 Structures of sildenafil (a), UK-103,320 (b), TPN729 (c), M3 (d), udenafil (e), and DA-8164 (f).

MATERIALS AND METHODS

Chemicals and reagents

TPN729 maleate (purity 99.92%) was supplied by Topfond Pharma Co., Ltd (Zhumadian China). Metabolite M3 (purity 98.7%) was synthesized by Vigonvita Life Science Co., Ltd (Suzhou, China). Sildenafil citrate (internal standard of TPN729, IS-1) was purchased from Sigma (St. Louis, MO, USA). TPN729M3-A (internal standard of M3, IS-2) was synthesized in-house. Ketoconazole (KET) and 1-aminobenzotriazole (ABT) were purchased from Meilun Biological Technology Co., Ltd (Dalian, China). Pooled human, monkey, dog, rat, mouse liver S9, microsomes, and human cytosol were obtained from Corning (NY, NY, USA). PDE5A was purchased from BPS Bioscience (San Diego, CA, USA). [^3H]-cGMP was purchased from PerkinElmer (Waltham, MA, USA).

HPLC grade acetonitrile and methanol were obtained from Merck (Darmstadt, Germany), while HPLC grade formic acid was supplied by TCI (Shanghai, China). A Milli-Q gradient water purification system (Millipore, Molsheim, France) was used to prepare HPLC grade water. Sodium chloride injection was supplied by Huayu Pharmaceutical Co., Ltd (Wuxi, China).

Monkey, dog, and rat pharmacokinetics

For the monkey pharmacokinetic study, three 5-year-old healthy male adult cynomolgus monkeys (weighing 3.2–4.2 kg) were provided by Jiangsu Tripod Preclinical Research Laboratories Co., Ltd (Nanjing, China). All monkeys were housed in separated cages and fed twice daily (at 09:00 and 15:00) with ad libitum access to water. The study protocol for monkey experiments was in accordance with the Guide for the Care and Use of Agricultural Animals in Research and Teaching, Association for Assessment and Accreditation of Laboratory Animal Care International. All cynomolgus monkeys were administered a nasogastric gavage dose of 5 mg/kg TPN729. Jugular vein blood collection (1 mL) was performed using $\text{K}_2\text{-EDTA}$ tubes at 0 (predose), 0.25, 0.5, 1, 1.5, 2, 4, 6, 8, and 24 h after dosing. After centrifugation at $3500 \times g$ for 10 min at 4 °C, the obtained plasma samples were stored at -20°C before liquid chromatography–tandem mass spectrometry (LC–MS/MS) analysis. After thawing and vortexing, the plasma concentrations of TPN729 and M3 were assessed following simple protein precipitation. Approximately 20 μL of plasma sample, 20 μL of IS, and 200 μL of acetonitrile were mixed, followed by vortexing for 1 min and centrifuging at $14,000 \times g$ for 5 min.

Subsequently, the mixture (2.5 μL) was subjected to LC–MS/MS detection.

For the dog pharmacokinetic study, three healthy male adult beagle dogs (1 year old, 10–15 kg) were provided by the Animal Center of Shanghai Institute of Materia Medica (SIMM), Chinese Academy of Sciences, China. All dogs were housed in separate cages and fed twice daily (at 08:00 and 19:00) with ad libitum access to water. The study protocol for dog experiments was in line with the guidelines approved by the Animal Care and Use Committee of SIMM. All beagle dogs were administered an oral gavage dose of 3 mg/kg TPN729. Jugular vein blood collection (1 mL) was performed using $\text{K}_2\text{-EDTA}$ tubes at 0 (predose), 0.25, 0.5, 1, 1.5, 2, 4, 6, 8, 24, and 48 h after dosing. After centrifugation at $3000 \times g$ for 10 min at 4 °C, the plasma samples were stored at -20°C before LC–MS/MS analysis.

For the rat pharmacokinetic study, eight male Sprague-Dawley (SD) rats (8–9 weeks old, 180–220 g) were kindly gifted by the Animal Center of SIMM. Animals were maintained in a specific pathogen-free area under a 12:12 h light–dark cycle at 25 °C and $50\% \pm 10\%$ humidity. All rats were given ad libitum access to food and water throughout the whole experiment. After 1 week of acclimatization, the rats were fasted overnight prior to the experiments. Ethical approval for the study protocol was obtained from the Animal Ethics Committee of SIMM, and the welfare of these rats was highly respected during the study. On day 1, the SD rats were administered an oral gavage dose of 5 mg/kg TPN729. Approximately 0.3 mL blood samples were collected from the posterior venous plexus using $\text{K}_2\text{-EDTA}$ tubes at 0 (predose), 0.25, 0.5, 1, 2, 4, 6, 10, and 24 h after dosing. After centrifugation at $11,000 \times g$ for 5 min at 4 °C, the plasma samples were stored at -20°C until detection. Sample preparations were conducted as described above.

Characterization of TPN729 metabolites in monkeys, dogs, and rats

The plasma samples of monkeys and dogs collected at 1.5 h in the pharmacokinetics assay were used for metabolite identification. Following 100 mg/kg dosing, three rat plasma samples were collected after 1.5 h in the same manner as described in the rat pharmacokinetics study. The same amounts (150 μL) of plasma samples were pooled from three monkeys, three dogs, and three rats. Subsequently, the pooled plasma was mixed with 300 μL of

acetonitrile and then vortexed for 1 min. After centrifugation at 12,000 × g for 5 min, the supernatant was transferred to a clean microcentrifuge tube and evaporated to dryness under nitrogen at 40 °C. The residue was reconstituted in 100 µL of acetonitrile and water (1:9, v/v). Then, UPLC/Q-TOF MS was used for metabolite identification.

In vitro incubation of TPN729 with human, monkey, dog, rat, and mouse liver S9

All incubations were carried out in triplicate at 37 °C, and the final volume of the mixture was 100 µL containing TPN729 (3 µM) and human/monkey/dog/rat/mouse liver S9 (2.0 mg protein/mL) in 100 mM phosphate-buffered saline (PBS, pH 7.4). Approximately 25 µL of 2 mM NADPH was added to initiate the reaction, followed by incubation for 60 min prior to termination with 100 µL of ice-cold acetonitrile. The inhibition study was carried out using the CYP3A-specific inhibitor KET (1 µM) and the nonspecific CYP inhibitor ABT (2 mM). These inhibitors were preincubated with TPN729-supplemented human, monkey, dog, rat, and mouse liver S9 at 37 °C for 5 min. After preincubation, the reactions were initiated with NADPH and quenched with 100 µL of ice-cold acetonitrile.

In vitro incubation of TPN729 with human, monkey, dog, rat, and mouse liver microsomes

All incubations were carried out in triplicate at 37 °C, and the final volume of the mixture was 100 µL containing TPN729 (3 µM) and human/monkey/dog/rat/mouse liver microsomes (0.5 mg protein/mL) in 100 mM PBS (pH 7.4). Incubation processes were conducted as described above.

In vitro incubation of TPN729 with human liver cytosol

Human liver cytosolic CYP-catalyzed oxidation was assessed in duplicate at 37 °C, and the final volume of the mixture was 100 µL containing TPN729 (10 µM) and human liver cytosol (2.0 mg protein/mL) in 100 mM PBS (pH 7.4). After preincubation for 3 min, 25 µL of NADPH (2 mM) was added to the mixture, and the mixture was incubated for 60 min prior to termination as described above.

PDE assays

Recombinant human PDE5A was used in the PDE assays. The inhibitory activities of TPN729 and M3 against PDE5A were evaluated as described previously [16].

Human plasma protein binding

TPN729 and M3 human plasma protein binding assays were conducted using a rapid equilibrium dialysis device (Thermo-Fisher Scientific, Waltham, MA, USA). The plasma concentrations of TPN729 and M3 were spiked in triplicate at 125 and 400 ng/mL, respectively. Plasma samples (100 µL) were loaded into the plasma chambers, whereas the buffer chambers were filled with 300 µL of PBS (pH 7.4). The plate was incubated for 6 h on an orbital shaker (250 rpm) at 37 °C in a CO₂ incubator (5% CO₂). The samples were then collected for the LC-MS/MS system.

The unbound fraction (f_u) in plasma was calculated from the ratio of the buffer chamber concentration (C_{receiver}) to the plasma chamber concentration (C_{donor}), and the plasma protein binding rate was calculated according to the second equation as follows:

$$f_u = C_{\text{receiver}}/C_{\text{donor}} \quad (1)$$

$$\text{Plasma protein binding rate} = (1 - f_u) \times 100\% \quad (2)$$

Instrumentation and conditions

Quantitative determination of TPN729 and M3 was performed using LC-MS/MS. A Shimadzu UPLC 30A System (Shimadzu, Kyoto, Japan) was used as the HPLC system. Mass spectrometric

determination was conducted using an AB5500 triple quadrupole instrument (AB Sciex, Ontario, Canada), while data processing was performed with Analyst 1.6.3 software (AB Sciex, Ontario, Canada). A Luna C8 column (50 × 2.0 mm, 5 µm; Phenomenex, LA, CA, USA) was used for chromatographic separation, which was maintained at 40 °C. The mobile phase employed in the gradient elution was comprised of 0.2% formic acid (A) and acetonitrile (B). The initial mobile phase was 20% B for 0.2 min, and then the concentration of B increased linearly to 80% over 0.7 min, followed by maintenance for 0.5 min. The initial mobile phase was used for column equilibration. The overall run time was 2.3 min, with a flow rate of 0.8 mL/min. The LC-MS/MS methods for the quantification of TPN729 and M3 have previously been validated, and the results are shown in Supplementary Data.

Analytes were measured using electrospray ionization (ESI) mass spectrometry in positive ion multiple reaction monitoring mode (MRM). The source temperature and ion spray voltage were set at 500 °C and 5500 V, respectively. The auxiliary, curtain, and nebulizer gas pressures were set at 50, 30, and 50 psi, respectively. Nitrogen was employed as the collision-activated dissociation gas at a pressure of 8 psi. For TPN729, the optimal MRM transition was m/z 517.3 → 325.2, and the collision energy and declustering potential were 46 and 86 V, respectively. For sildenafil, the internal standard was TPN729, the optimal MRM transition was m/z 475.1 → 100.2, and the collision energy and declustering potential were 37 and 78 V, respectively. For M3, the optimal MRM transition was m/z 420.1 → 283.1, and the collision energy and declustering potential were 45 and 50 V, respectively. For TPN729M3-A, the internal standard of M3, the optimal MRM fragmentation transition was m/z 434.1 → 299.3, and the collision energy and declustering potential were 90 and 45 V, respectively. The overall scanning time was 30 ms.

The HR-MS and HR-MS² analyses were conducted on an Acquity UPLC system coupled to a Synapt G2 quadrupole time-of-flight (Q-TOF) mass spectrometer (Waters Corporation, Milford, MA, USA) equipped with a standard ESI source. The chromatographic conditions and mass spectrometric conditions were the same as those previously published [12].

Data analysis

The pharmacokinetic parameters of TPN729 and M3 were calculated by WinNonlin version 6.4 (Pharsight Corporation, Mountain View, LA, CA, USA) using a noncompartmental model. In the PDE assay, IC₅₀ values were calculated from the concentration-inhibition curve by nonlinear regression analysis using GraphPad Prism 8.0 (GraphPad Software, Inc, San Diego, CA, USA).

RESULTS

Metabolite profiling and pharmacokinetic evaluation of TPN729 and M3 in monkeys, dogs, and rats

Metabolite profiling and pharmacokinetic evaluation of TPN729 and M3 in monkeys. Monkey metabolite profiling is presented in Fig. 2a, and the plasma concentration-time curves of TPN729 and M3 are plotted in Fig. 2b. The main pharmacokinetic parameter ratios of M3 to TPN729 are presented in Table 1. Both TPN729 and M3 peaked at 1.0 h after dosing. The C_{max} values of TPN729 and M3 were 34.6 and 168 ng/mL, respectively, while the AUC_{0-∞} values were 94.0 and 329 ng·h/mL, respectively. The half-lives of TPN729 and M3 were 2.0 and 1.1 h, respectively. The pharmacokinetic results demonstrated that the plasma exposure of metabolite M3 was 3.5-fold higher than that of TPN729. The main metabolites detected in monkey plasma were dealkylation metabolite M3 and pyrrolidine lactam metabolite M11-2.

Metabolite profiling and pharmacokinetic evaluation of TPN729 and M3 in dogs. Dog metabolite profiling is presented in Fig. 2c, and the plasma concentration-time curves of TPN729 and M3

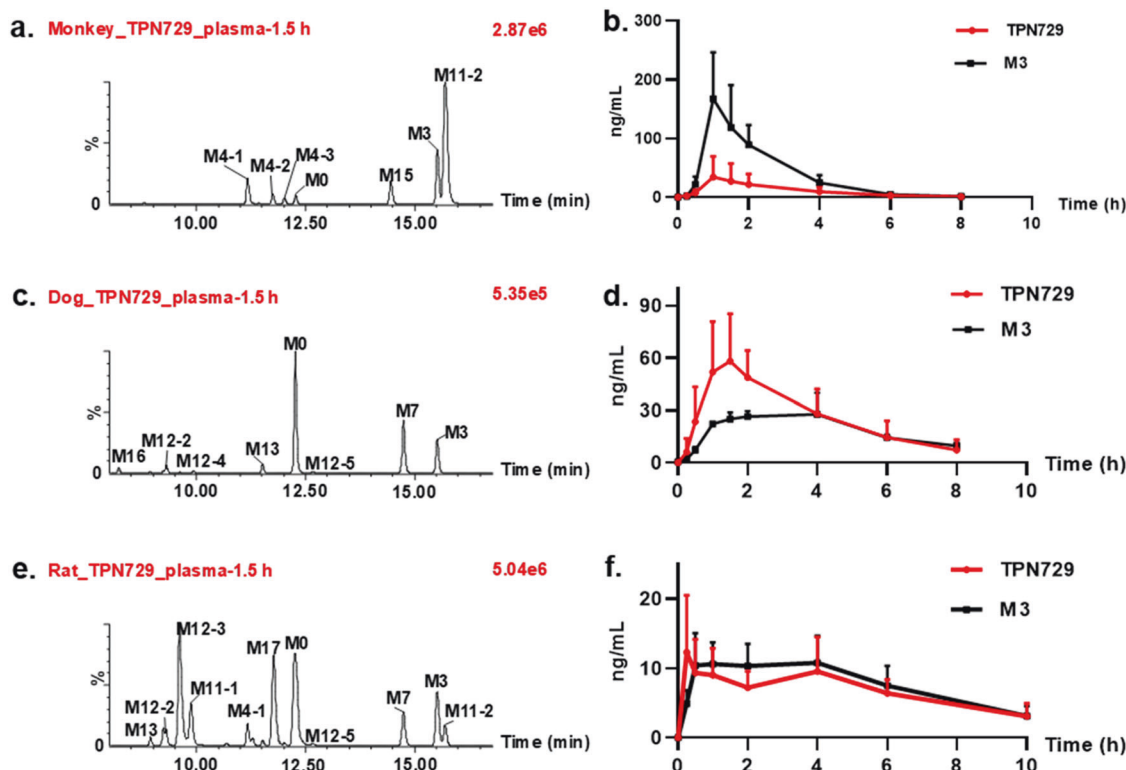


Fig. 2 Metabolic profile and pharmacokinetics of TPN729 in different species: monkey plasma at 1.5 h (a), monkey pharmacokinetics (b), dog plasma at 1.5 h (c), dog pharmacokinetics (d), rat plasma at 1.5 h (e), and rat pharmacokinetics (f).

Table 1. Mean pharmacokinetic parameter ratios of M3 to TPN729 in human [15], monkey, dog and rat plasma after single dose of 25, 5, 3 and 5 mg/kg TPN729 ($n = 3, 3, 3$ and 8, respectively).

Parameter ratio	Human	Monkey	Dog	Rat
$C_{\max} \text{ M3}/C_{\max} \text{ TPN729}$	3.49	4.86	0.54	0.90
$AUC_{(0-t)} \text{ M3}/AUC_{(0-t)} \text{ TPN729}$	6.93	3.71	1.23	1.15
$AUC_{(0-\infty)} \text{ M3}/AUC_{(0-\infty)} \text{ TPN729}$	7.57	3.50	1.15	1.11

Data have been combined for other parameters, thus preventing statistical analysis

C_{\max} maximum plasma concentration

$AUC_{(0-t)}$ area under the concentration–time curve from time 0 extrapolated until the end of the dosing interval

$AUC_{(0-\infty)}$ area under the concentration–time curve from time 0 extrapolated to infinity

are illustrated in Fig. 2d. The main pharmacokinetic parameter ratios of M3 to TPN729 are described in Table 1. TPN729 and M3 concentrations peaked at 1.33 and 2.50 h after dosing, respectively. The C_{\max} values of TPN729 and M3 were 58.3 and 31.3 ng/mL, respectively, while the $AUC_{0-\infty}$ values were 242 and 278 ng·h/mL, respectively. The half-lives of TPN729 and M3 were 1.94 and 7.85 h, respectively. The pharmacokinetic results demonstrated that the plasma exposure of metabolite M3 was 1.2-fold higher than that of TPN729. The main metabolites found in dog plasma were dealkylation metabolite M3 and pyrrolidine oxidative deamination metabolite M7.

Metabolite profiling and pharmacokinetic evaluation of TPN729 and M3 in rats. Rat metabolite profiling is presented in Fig. 2e, and the plasma concentration–time curves of TPN729 and M3 are plotted in Fig. 2f. The main pharmacokinetic parameter ratios of M3 to TPN729 are presented in Table 1. TPN729 and M3

concentrations peaked at 1.72 and 2.50 h, respectively. After dosing, the C_{\max} values of TPN729 and M3 were 14.4 and 12.9 ng/mL, respectively, while the $AUC_{0-\infty}$ values were 73.7 and 81.9 ng·h/mL, respectively. The pharmacokinetic results indicated that the plasma exposure of metabolite M3 was 1.1-fold higher than that of TPN729. The main metabolites detected in rat plasma were monooxidative metabolite M12-3 and depropyl metabolite M17.

In our laboratory, the pharmacokinetics and identification of TPN729 in humans have been studied previously. The findings revealed that the plasma exposure of M3 in humans was 7.6-fold higher than that of TPN729 [15]. Moreover, a total of 22 metabolites were identified, seven of which were confirmed by comparison with the reference substances [12]. Through the use of the identification method established in humans, the main metabolites in monkeys, dogs, and rats were characterized according to their fragment ions and retention time (Tables S1 and S2). The main proposed metabolic pathways of TPN729 in different species are illustrated in Fig. 3. Apart from the 22 metabolites identified previously, new metabolites (M15–M17) were speculated in monkeys, dogs, and rats based on their fragment ions, and the details of their characterization are presented in Supplementary Data.

Metabolism of TPN729 in liver S9 of different species

The incubation results in the liver S9 of different species are presented in Fig. 4. As shown in Fig. 4a, the incubation system without NADPH was set as the control group, and the remaining amount of TPN729 in the S9 of different species was ~1500 nM. As shown in Fig. 4b, after 1 h of incubation with TPN729, the remaining amounts of TPN729 were 400, 16.1, 1193, 119, and 199 nM in the liver S9 of humans, monkeys, dogs, rats, and mice, respectively. As shown in Fig. 4c, after the addition of 1 μM CYP3A-specific inhibitor KET into the S9 incubation system, the remaining amounts of TPN729 were 1396, 836, 1330, 367, and 401 nM in the liver S9 of humans, monkeys, dogs, rats, and mice, respectively. As

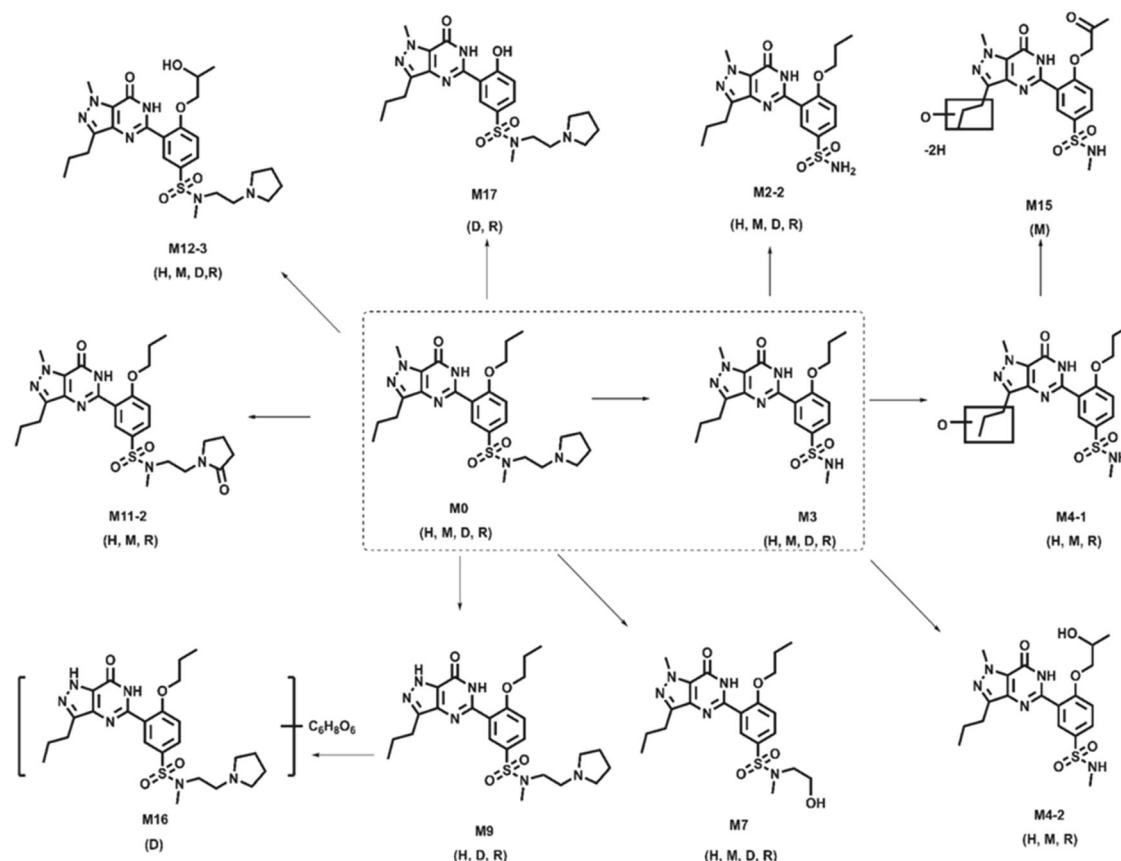


Fig. 3 Proposed main metabolic pathways in humans (H), monkeys (M), dogs (D) and rats (R).

shown in Fig. 4d, after the addition of 2 mM nonspecific CYP3A inhibitor ABT, the remaining amounts of TPN729 were 1506, 1603, 1420, 1350, and 1290 nM in the liver S9 of humans, monkeys, dogs, rats, and mice, respectively. The results showed that the metabolism of TPN729 in different species of liver S9 was relatively different. TPN729 was poorly metabolized in dog liver S9, moderately metabolized in human liver S9, and almost completely metabolized in monkey liver S9. KET and ABT almost entirely inhibited the metabolism of TPN729 in human liver S9 but only partially inhibited the metabolism in monkey, rat, and mouse liver S9. As shown in Fig. 4e, the levels of M3 in human and monkey liver S9 were 410 and 151 nM, respectively. This was followed by 23.0, 52.4, and 69.1 nM in the liver S9 of rats, dogs, and mice, respectively. Our results indicated that the amounts of M3 formation were relatively similar in humans and monkeys, which were much higher than those in the other species. As shown in Fig. 4f, after incubation with KET (a CYP3A-specific inhibitor), the levels of M3 were 7.1, 179, 1.2, 37.8, and 37.9 in liver S9 of humans, monkeys, dogs, rats, and mice, respectively. M3 could not be generated in the presence of ABT (Fig. 4g), indicating that CYP3A was not involved in the formation of M3 in monkeys.

TPN729 metabolism in the liver microsomes of different species
 The incubation results in the liver microsomes of different species are presented in Fig. 5. As shown in Fig. 5a, the incubation system without NADPH was set as the control group. After 1 h of incubation with TPN729, the remaining amounts of TPN729 were 474, 28.2, 822, 193, and 77.9 nM in the liver microsomes of humans, monkeys, dogs, rats, and mice, respectively (Fig. 5b). After the addition of 1 μ M CYP3A-specific inhibitor KET to the microsomal incubation system, the remaining amounts of TPN729 were 1593, 639, 1290, 47.1, and 14.9 nM in the liver microsomes of humans, monkeys, dogs, rats, and mice, respectively (Fig. 5c). After

the addition of 2 mM nonspecific CYP3A inhibitor ABT, the remaining amounts of TPN729 were 1683, 1640, 1330, 1247, and 1410 nM in the liver microsomes of humans, monkeys, dogs, rats, and mice, respectively (Fig. 5d). These results indicate that the hepatic microsomal metabolism of TPN729 is relatively different in humans and other species. Similar to the liver S9 of various species, TPN729 was poorly metabolized in the liver microsomes of dogs, and KET almost entirely inhibited the metabolism of TPN729 in human liver microsomes but not in the liver microsomes of monkeys, rats, and mice. As shown in Fig. 5e, the levels of M3 in human and monkey liver microsomes were 217 and 148 nM, respectively. This was followed by 70.8, 32.6, and 7.2 nM in the liver microsomes of rats, dogs, and mice, respectively. As shown in Fig. 5f, after incubation with KET, the levels of M3 were 3.4, 151, 2.1, 36.8, and 4.3 in liver microsomes of humans, monkeys, dogs, rats, and mice, respectively. The results in microsomes were consistent with those in liver S9. Furthermore, our data revealed that M3 could not be detected in the human liver cytosol following the addition of NADPH.

PDE5A inhibitory activity

The IC_{50} values of TPN729 and M3 for PDE5A were 6.17 ± 0.48 and 7.94 ± 0.07 nM, respectively. The results of the inhibitory activity are shown in Fig. 6.

Plasma protein binding results

The unbound fraction (f_u) values of TPN729 and M3 were determined to be 0.073 and 0.013, respectively; therefore, their plasma protein binding rates were 92.7% and 98.7%, respectively (Figs. S1 and S2). The plasma exposure of M3 in humans was 7.6-fold higher than that of TPN729, the inhibitory activity of M3 against PDE5 was 0.78-fold that of TPN729, and the unbound fraction of M3 in human plasma was 0.18-fold that of TPN729. This

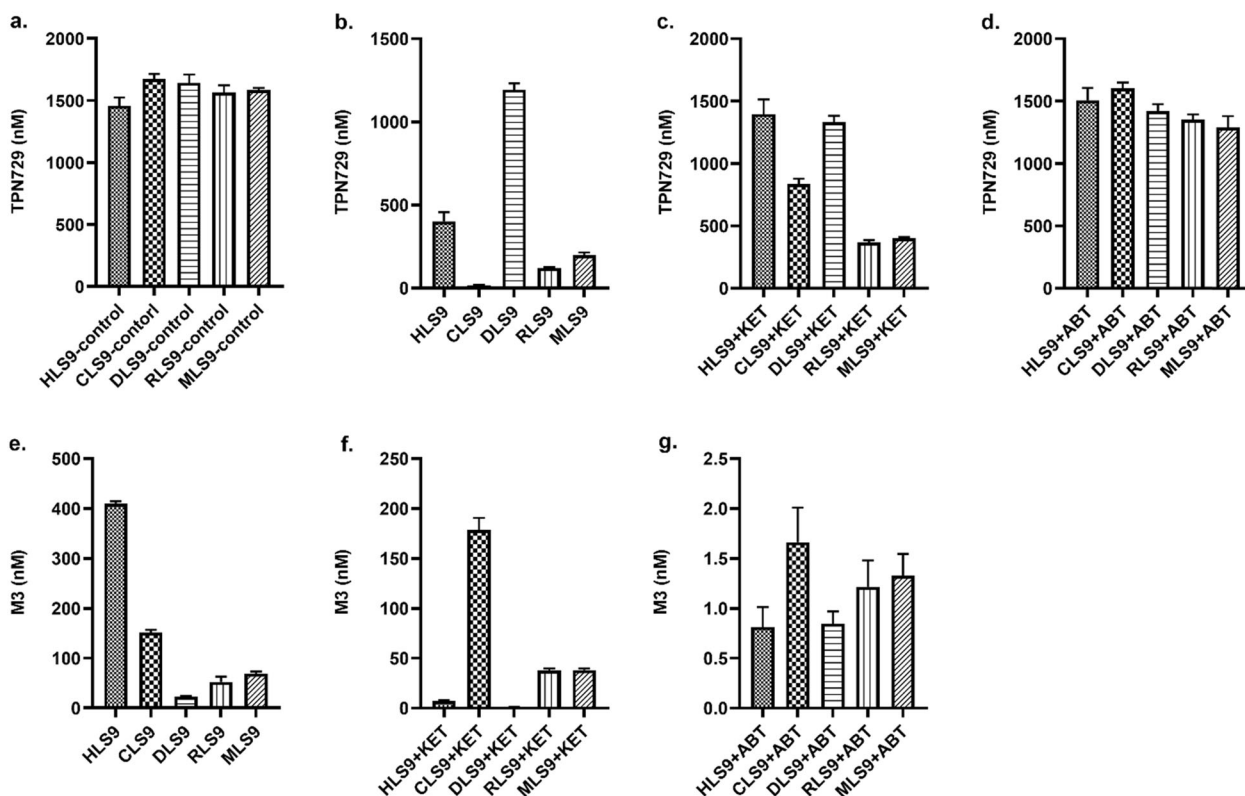


Fig. 4 TPN729 residues and M3 formation in the liver S9 of different species (humans (H), cynomolgus monkeys (C), dogs (D), rats (R), and mice (M)): incubation without NADPH as a negative control (a), S9 normal incubation (b), S9 incubation with KET (c), S9 incubation with ABT (d), M3 formation in normal incubation (e), M3 formation with KET (f), and M3 formation with ABT (g).

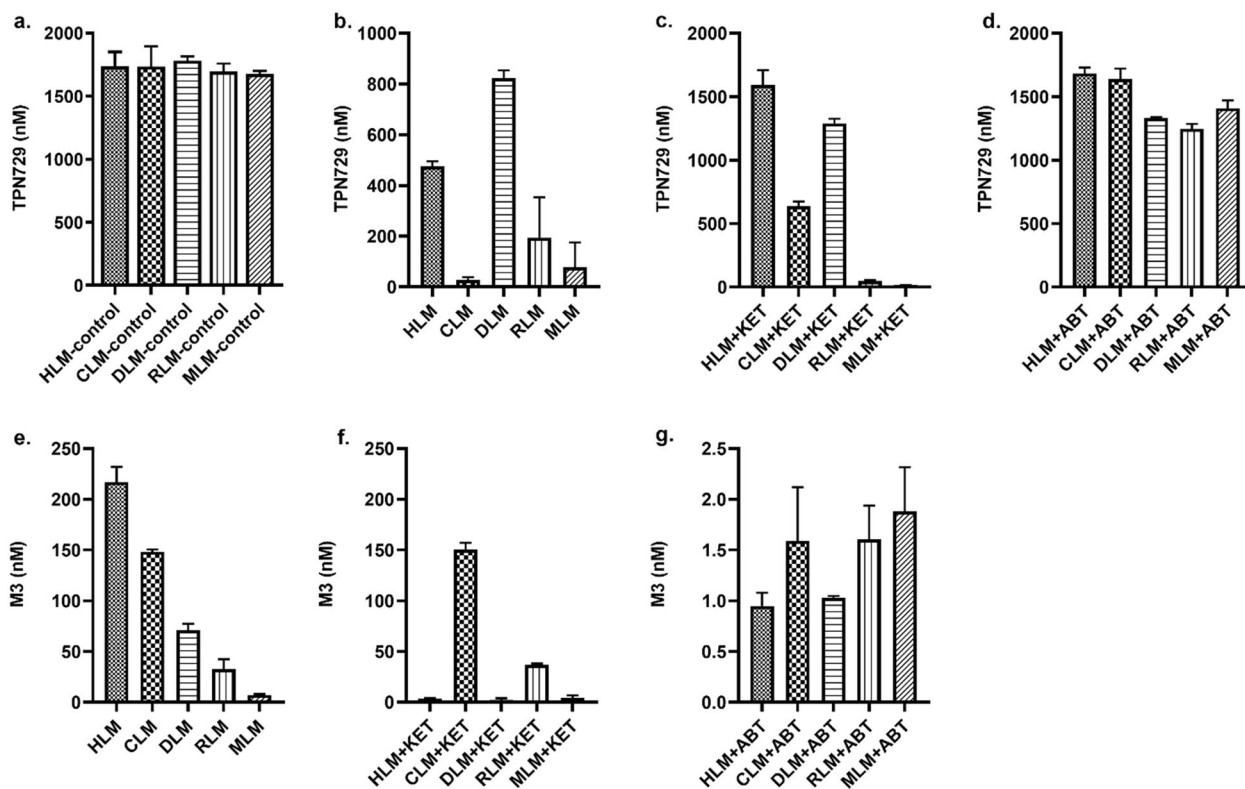


Fig. 5 TPN729 residues and M3 formation in the liver microsomes of different species: incubation without NADPH as a negative control (a), normal microsome incubation (b), microsome incubation with KET (c), microsome incubation with ABT (d), M3 formation in normal incubation (e), M3 formation with KET (f), and M3 formation with ABT (g).

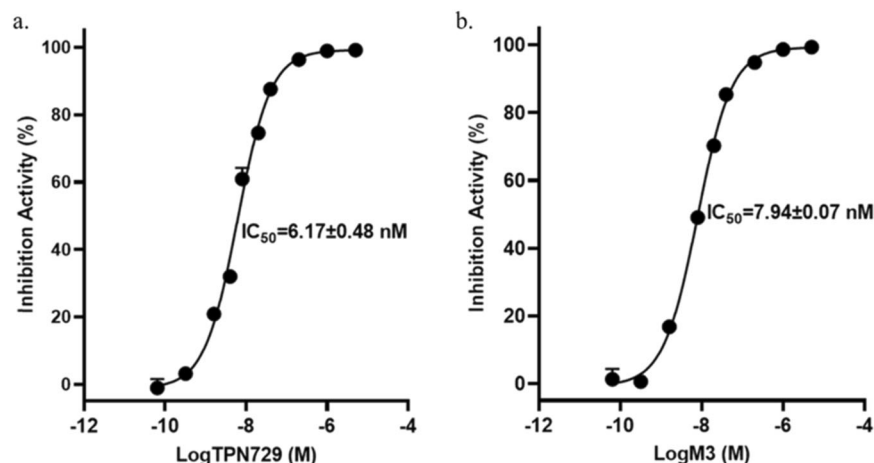


Fig. 6 Inhibitory activities of TPN729 (a) and M3 (b) against PDE5.

indicates that the pharmacological contribution of M3 is relatively similar to that of TPN729 in humans.

DISCUSSION

The metabolism and pharmacokinetics of TPN729 exhibited great species differences, and the exposure of M3 was 7.6-fold greater than that of TPN729 in humans [15], 3.5-fold greater than that in monkeys, 1.2-fold greater than that in dogs, and 1.1-fold greater than that in rats. The *in vitro* incubation results with TPN729 suggest that CYP3A4 is the cause of species differences. Further studies showed that M3 was an active metabolite, and its pharmacological contribution was similar to that of TPN729. Considering that CYP3A4 is the most important enzyme in the human body, the species differences of the CYP3A4 enzyme could be of great significance for selecting an appropriate animal model to predict clinical pharmacokinetics and evaluate drug efficacy and toxicity.

Numerous studies have investigated the species differences in CYP3A4 metabolism. In some cases, animal models can be used to evaluate the metabolism of some drugs metabolized by CYP3A4. For example, sildenafil is primarily metabolized by CYP3A4, and the metabolism of sildenafil in mice is highly analogous compared with that in other animals [7]. GLS4 is an active substrate of CYP3A, and GLS4 metabolites are relatively comparable in the CYP3A4 microsomes of dogs and humans [17]. Beagle dogs can be chosen as an animal model to evaluate Sly930 metabolism in humans [18]. In addition, slight differences were observed in the metabolism of dictamnine in mouse, rat, dog, monkey, and human microsomes [19]. Delamanid metabolites catalyzed by CYP3A4 are found in humans and dogs to a greater extent than those found in rodents [20]. 20(S)-Ginsenoside Rh2 metabolism was evaluated in the liver microsomes of humans, monkeys, dogs, rats, and mice, and no significant differences were observed in the phase I metabolic profile among the five tested species [21]. In other cases, animal models are not suitable to predict human CYP3A4-mediated metabolism of certain drug candidates. For example, CYP3A4 plays a predominant role in the hydroxylation reaction of 11-keto- β -boswellic acid; however, deacetylation and regioselective hydroxylation exhibit considerable species differences [22]. The overall metabolic fingerprint of lasiocarpine detected with human liver microsomes may differ from that in other species [23]. In rat, dog, and human liver microsomes, the mycotoxin enniatin B exhibited considerable species differences in the bioformation rate and metabolite patterns [24]. It is important to realize that humans differ from animals with regard to the isoform composition, expression, and catalytic activities of drug-metabolizing enzymes. Notably, the species-specific isoforms of CYPs 1A, 2C, 2D,

and 3A show appreciable interspecies differences in terms of catalytic activity, and thus, some caution should be applied when extrapolating metabolism data from animal models to humans [25]. As a result, the species differences in CYP3A metabolism are difficult to predict, which need to be verified by experiments on a case by case basis. In our study, we found that the catalytic ability of CYP3A to form M3 was completely different in humans and monkeys.

Cynomolgus monkeys can be an appropriate animal model to evaluate the safety and efficacy of TPN729 in humans. The reasons are as follows: (1) the metabolic pathways of cynomolgus monkeys are consistent with those of humans, while those of dogs and rats are relatively similar (the main metabolites of TPN729 in humans and monkeys are M3 and M11-2, whereas M7, M12-3, and M17 are the major metabolites in dogs and rats). (2) With regard to the plasma concentration and exposure of TPN729 and M3, the similarity between monkeys and humans is much higher compared with humans and dogs and humans and rats. Although the cDNA and amino acids of the cynomolgus monkey CYP3A enzyme show up to 90% homology with the human CYP3A enzyme and the tissue expression and catalytic activity of CYP3A are relatively similar [26–28], the catalytic capacity of CYP3A on the formation of M3 in humans and monkeys was quite different. However, based on pharmacokinetic studies and metabolite profiles in humans and monkeys, cynomolgus monkeys may serve as the most suitable animal model for investigating TPN729 metabolism.

TPN729 has the same pharmacological effects as sildenafil. These compounds are structurally similar and primarily metabolized by CYP3A. However, the metabolic pathways and metabolites produced by TPN729 and sildenafil are vastly different. Sildenafil is primarily metabolized by CYP3A to produce the more polar metabolite N-desmethylsildenafil [7, 8, 15, 29, 30]. However, according to the calculated data of Advanced Chemistry Development (ACD/Labs) software (Percepta 2018.1), TPN729 was stripped of the alkaline tetrahydropyrroethyl group to form M3, and their logD values were -0.4 and 1.72 in the stomach, -0.26 and 1.86 in the duodenum, and 0.7 and 1.85 in the blood, respectively. Combined with the elution time of M3 (later than that of TPN729) by HPLC, it was obvious that M3 was a less polar metabolite, which was not common after general oxidative metabolism. However, the safety of M3 has not been evaluated before. According to the guidelines for metabolite safety assessment [31], a corresponding safety assessment of the TPN729 metabolite M3 should be performed.

TPN729 is an isomer of udenafil, and their main metabolites, M3 and DA-8164, respectively, were similar in structure with the difference of a methyl group. The pharmacological contribution of

DA-8164 as a PDE5 inhibitor is half that of udenafil [11], while the contribution of M3 is equal to that of TPN729. The ratio of $AUC_{DA-8164}/AUC_{udenafil}$ in humans is 1.39 [11], while the ratio of AUC_{M3}/AUC_{TPN729} is 7.6. CYP3A4 is mainly responsible for the metabolism of TPN729 and udenafil [10]. The half-lives of TPN729 and M3 are 10.6 and 11.8 h, and their peak times are 2.33 and 2.50 h [15], respectively. It is worth noting that TPN729 and udenafil share similar metabolic pathways. However, the relative exposure of metabolite M3 is much higher than that of DA-8164.

In our study, the proportions of M3 formation were inconsistent in S9 and microsomes of different species. In liver S9 and microsomes, the amount of M3 was the highest among humans and monkeys (humans > monkeys), and the order was mice > rats > dogs in the other species in S9, while in liver microsomes, the order was dogs > rats > mice. The results indicated that the catalytic capabilities of liver S9 and microsomes are different. Each in vitro model has its own advantages and limitations. S9 contains both microsomal and cytosolic fractions, expressing more types of enzymes, but the content of these enzymes is ~20%–25% of the corresponding microsomal fraction [32].

At present, a wide variety of CYP3A4 inducers and inhibitors has been used in clinical practice. Moreover, CYP3A4 accounted for 70% of TPN729 metabolism and 93.6% of M3 formation [15]. Therefore, the drug–drug interaction potential of TPN729 mediated by CYP3A4 should be taken into consideration in clinical practice.

CONCLUSION

In conclusion, CYP3A4 caused a seven-fold difference in the formation of M3 in diverse species. The plasma exposure of M3 was 7.6-fold higher than that of TPN729 in humans [15], and M3 exhibited the same pharmacological contribution as TPN729. Therefore, more attention should be paid to the limitations and selection of animal models for predicting the clinical pharmacokinetics of drug candidates metabolized by CYP3A4.

ACKNOWLEDGEMENTS

This study was supported by the National Natural Science Foundation of China (Nos 81521005 and 81903701) and the Strategic Priority Research Program of the Chinese Academy of Sciences (No. XDA12050306). The authors thank Jia-lan Zhou and Wei Li for their assistance with the experiments.

AUTHOR CONTRIBUTIONS

QQT, YTX, XXD, XLZ, YCX, XRJ, JSS, ZW, and DFZ were responsible for the research design, data analysis, and writing of the paper; QQT and XLZ performed experiments.

ADDITIONAL INFORMATION

The online version of this article (<https://doi.org/10.1038/s41401-020-0447-x>) contains supplementary material, which is available to authorized users.

Competing interests: The authors declare no competing interests.

REFERENCES

- Allen MS, Walter EE. Erectile dysfunction: an umbrella review of meta-analyses of risk-factors, treatment, and prevalence outcomes. *J Sex Med.* 2019;16:531–41.
- Lotti F, Maggi M. Sexual dysfunction and male infertility. *Nat Rev Urol.* 2018;15:287–307.
- Andersson KE. PDE5 inhibitors—pharmacology and clinical applications 20 years after sildenafil discovery. *Br J Pharmacol.* 2018;175:2554–65.
- Wang Z, Zhu DF, Yang XC, Li JF, Jiang XR, Tian GH, et al. The selectivity and potency of the new PDE5 inhibitor TPN729MA. *J Sex Med.* 2013;10:2790–7.
- Warrington JS, Shader RI, von Moltke LL, Greenblatt DJ. In vitro biotransformation of sildenafil (Viagra): identification of human cytochromes and potential drug interactions. *Drug Metab Dispos.* 2000;28:392–7.

- Warrington JS, von Moltke LL, Hartz JS, Shader RI, Greenblatt DJ. The effect of age on sildenafil biotransformation in rat and mouse liver microsomes. *Drug Metab Dispos.* 2003;31:1306–9.
- Lee SK, Kim DH, Yoo HH. Comparative metabolism of sildenafil in liver microsomes of different species by using LC/MS-based multivariate analysis. *J Chromatogr B Anal Technol Biomed Life Sci.* 2011;879:3005–11.
- Walker DK, Ackland MJ, James GC, Muirhead GJ, Rance DJ, Wastall P, et al. Pharmacokinetics and metabolism of sildenafil in mouse, rat, rabbit, dog and man. *Xenobiotica.* 1999;29:297–310.
- Cho YS, Noh YH, Lim HS, Cho SH, Ghim JL, Choe S, et al. Effects of renal impairment on the pharmacokinetics and safety of udenafil. *J Clin Pharmacol.* 2018;58:905–12.
- Ji HY, Lee HW, Kim HH, Kim DS, Yoo M, Kim WB, et al. Role of human cytochrome P450 3A4 in the metabolism of DA-8159, a new erectogenic. *Xenobiotica.* 2004;34:973–82.
- Shim HJ, Kim YC, Lee JH, Park KJ, Kwon JW, Kim WB, et al. Species differences in the formation of DA-8164 after intravenous and/or oral administration of DA-8159, a new erectogenic, to mice, rats, rabbits, dogs and humans. *Biopharm Drug Dispos.* 2005;26:161–6.
- Zhu YT, Li L, Deng P, Chen XY, Zhong DF. Characterization of TPN729 metabolites in humans using ultra-performance liquid chromatography/quadrupole time-of-flight mass spectrometry. *J Pharm Biomed Anal.* 2016;117:217–26.
- Liu Y, Shao SG, Song HL, Yao XT, Liu J, Liu HZ, et al. Simultaneous determination of TPN729 and its five metabolites in human plasma and urine by liquid chromatography coupled to tandem mass spectrometry. *J Pharm Biomed Anal.* 2018;151:91–105.
- Gao ZW, Zhu YT, Yu MM, Zan B, Liu J, Zhang YF, et al. Preclinical pharmacokinetics of TPN729MA, a novel PDE5 inhibitor, and prediction of its human pharmacokinetics using a PBPK model. *Acta Pharmacol Sin.* 2015;36:1528–36.
- Zhu YT. Study on the metabolism, pharmacokinetics, drug-drug interaction, and multidrug resistance reversal effect of TPN729. Dissertation, Chinese Academy of Science University. Beijing, 2017.
- Wang Z, Jiang XR, Zhang XL, Tian GH, Yang RL, Wu JZ, et al. Pharmacokinetics-driven optimization of 4(3H)-pyrimidinones as phosphodiesterase type 5 inhibitors leading to TPN171, a clinical candidate for the treatment of pulmonary arterial hypertension. *J Med Chem.* 2019;62:4979–90.
- Zhou X, Gao ZW, Meng J, Chen XY, Zhong DF. Effects of ketoconazole and rifampicin on the pharmacokinetics of GL54, a novel anti-hepatitis B virus compound, in dogs. *Acta Pharmacol Sin.* 2013;34:1420–6.
- Mi JQ, Zhao MM, Yang S, Jia YF, Wang Y, Wang BL, et al. Identification of cytochrome P450 isoforms involved in the metabolism of Syl930, a selective S1PR(1) agonist acting as a potential therapeutic agent for autoimmune encephalitis. *Drug Metab Pharmacokinet.* 2017;32:53–60.
- Wang P, Zhao YL, Zhu YD, Sun JB, Yerke A, Sang SM, et al. Metabolism of diltiazem in liver microsomes from mouse, rat, dog, monkey, and human. *J Pharm Biomed Anal.* 2016;119:166–74.
- Sasahara K, Shimokawa Y, Hirao Y, Koyama N, Kitano K, Shibata M, et al. Pharmacokinetics and metabolism of delamanid, a novel anti-tuberculosis drug, in animals and humans: importance of albumin metabolism in vivo. *Drug Metab Dispos.* 2015;43:1267–76.
- Li L, Chen XY, Zhou JL, Zhong DF. In vitro studies on the oxidative metabolism of 20(S)-ginsenoside Rh2 in human, monkey, dog, rat, and mouse liver microsomes, and human liver S9. *Drug Metab Dispos.* 2012;40:2041–53.
- Cui YL, Tian XG, Ning J, Wang C, Yu ZL, Wang Y, et al. Metabolic profile of 3-acetyl-11-keto-beta-boswellic acid and 11-keto-beta-boswellic acid in human preparations in Vitro, species differences, and bioactivity variation. *AAPS J.* 2016;18:1273–88.
- Fashe MM, Juvonen RO, Petsalo A, Rasanen J, Pasanen M. Species-specific differences in the in vitro metabolism of lasiocarpine. *Chem Res Toxicol.* 2015;28:2034–44.
- Faeste CK, Ivanova L, Uhlig S. In vitro metabolism of the mycotoxin enniatin B in different species and cytochrome P450 enzyme phenotyping by chemical inhibitors. *Drug Metab Dispos.* 2011;39:1768–76.
- Martignoni M, Groothuis GMM, de Kanter R. Species differences between mouse, rat, dog, monkey and human CYP-mediated drug metabolism, inhibition and induction. *Expert Opin Drug Metab Toxicol.* 2006;2:875–94.
- Uehara S, Uno Y, Nakanishi K, Ishii S, Inoue T, Sasaki E, et al. Marmoset cytochrome P450 3A4 ortholog expressed in liver and small-intestine tissues efficiently metabolizes midazolam, alprazolam, nifedipine, and testosterone. *Drug Metab Dispos.* 2017;45:457–67.
- Uehara S, Murayama N, Nakanishi Y, Zeldin DC, Yamazaki H, Uno Y. Immunohistochemical detection of cytochrome P450 enzymes in liver microsomes of 27 cynomolgus monkeys. *J Pharmacol Exp Ther.* 2011;339:654–61.

28. Ohtsuka T, Yoshikawa T, Kozakai K, Tsuneto Y, Uno Y, Utoh M, et al. Alprazolam as an in vivo probe for studying induction of CYP3A in cynomolgus monkeys. *Drug Metab Dispos.* 2010;38:1806–13.
29. Muirhead GJ, Rance DJ, Walker DK, Wastall P. Comparative human pharmacokinetics and metabolism of single-dose oral and intravenous sildenafil citrate. *Br J Clin Pharmacol.* 2002;53:135–205.
30. Ku HY, Ahn HJ, Seo KA, Kim H, Oh M, Bae SK, et al. The contributions of cytochromes P450 3A4 and 3A5 to the metabolism of the phosphodiesterase type 5 inhibitors sildenafil, udenafil, and vardenafil. *Drug Metab Dispos.* 2008;36:986–90.
31. Schadt S, Bister B, Chowdhury SK, Funk C, Hop C, Humphreys WG, et al. A decade in the MIST: learnings from investigations of drug metabolites in drug development under the “Metabolites in Safety Testing” regulatory guidance. *Drug Metab Dispos.* 2018;46:865–78.
32. Jia L, Liu XD. The conduct of drug metabolism studies considered good practice (II): in vitro experiments. *Curr Drug Metab.* 2007;8:822–9.